

A polarity-induced defect mechanism for conductivity and magnetism at polar-nonpolar oxide interfaces

Liping Yu and Alex Zunger

University of Colorado, Boulder, Colorado 80309, USA

The discovery of conducting two-dimensional electron gas (2DEG) and magnetism at the interface between insulating nonmagnetic oxides, as exemplified by the polar LaAlO₃ and nonpolar SrTiO₃ has raised prospects for attaining interfacial functionalities absent in the component materials. Yet, the microscopic origin of such emergent phenomena remains unclear, posing obstacles to design of improved functionalities. Using first principles defect calculations, we reveal a unifying polarity-induced defect mechanism for both conductivity and magnetism at polar-nonpolar interfaces of nonmagnetic insulating oxides. We demonstrate that the polar-discontinuity across the interface triggers thermodynamically the spontaneous formation of certain defects that in turn cancel the polar field induced by the polar discontinuity. It turns out that the 2DEG originates from those spontaneously formed surface donor defects (oxygen vacancy), but the density of 2DEG is controlled by the interfacial anti-site acceptor defects (Al-on-Ti). The interface magnetism is found to originate from the un-ionized deep Ti-on-Al anti-site donor defects within the LaAlO₃ side near the interface. Our results suggest practical design guidelines for inducing and controlling both 2DEG and magnetism at polar-nonpolar oxide interfaces.

Oxide interfaces exhibit many spectacular phenomena not found in the respective bulk components or in conventional semiconductor interfaces¹, providing new avenues for electronics². The LaAlO₃/SrTiO₃ interface is a paradigm example, exhibiting conducting 2DEG^{3,4} and magnetism⁵⁻¹¹ between two insulating nonmagnetic metal-oxides. In the [001] direction, two different interfaces can be formed between polar LaAlO₃, which consists of alternating LaO⁺-(AlO₂)⁻ layers, and nonpolar SrTiO₃, which consists of alternating (SrO)⁰-(TiO₂)⁰ layers. One is called n-type (i.e., LaO/TiO₂) and the other is called p-type (i.e., AlO₂/SrO). The remarkable feature is that the conductivity occurs only at n-type interfaces when the LaAlO₃ film thickness (n_{LAO}) is larger than three unit cells (uc)^{4,5}, whereas the magnetism has been observed both at n-type interfaces with $n_{LAO} > \sim 3$ uc and at insulating p-type interfaces⁸. As listed in Table 1, this feature and other experimental observations represent the main puzzles¹² that need to be resolved before the promised applications can be realized¹³.

Existing explanations: At present, no single mechanism can fully explain the vast and growing body of experimental work on this LaAlO₃/SrTiO₃ system. *For 2DEG at n-type interfaces*, four main mechanisms have been suggested. The prevalent one is intrinsic electronic reconstruction (so called polar catastrophe) involving ionization of the host valence band of LaAlO₃ within the abrupt and defect-free interfaces^{3,4}. The other three mechanisms involve various defects, including the oxygen vacancies at the interface (denoted as $V_O(I)$, where “I” means *Interface*)¹⁴⁻¹⁶, oxygen vacancies at LaAlO₃ overlayer surface (denoted as $V_O(S)$, where *S* means *Surface*)¹⁷⁻²², and the La-on-Sr (La_{Sr}) antisite donor defects induced by interfacial cation intermixing²³⁻²⁹. As Table 1 shows, each mechanism represents one aspect of the interface physics, explains some experimental findings, but conflicts with a few others². None explains the insulating nature of p-type interfaces. *For interface magnetism*, it was shown experimentally that the local magnetic moments are associated with Ti³⁺ ions^{5-11,30}. However, it is yet unclear whether such Ti³⁺ ions reside in SrTiO₃, or LaAlO₃, or both near the interface. Theoretically, it has been postulated that Ti³⁺ ions arise in SrTiO₃ side, involving the occupation of the low-energy Ti- d_{xy} -like sub-bands caused by the interfacial splitting of orbital degeneracy³¹, or interfacial

disorder^{32,33}, or interfacial oxygen vacancies³⁴, which are difficult to reconcile why the magnetism appears at insulating p-type interfaces and at n-type interfaces with a critical thickness (L_c) similar to that for 2DEG.

Overarching unresolved questions: a crucial issue associated with the emergent conductivity and magnetism at polar-nonpolar interfaces is what mitigates the divergence of electrostatic potential as the thickness of the polar film increases³⁵. Is it electronic reconstruction within polar catastrophe scenario, atomic reconstruction, or chemical defects? Different answer represents different mechanism, suggesting different controlling parameters. It has been purported that all these three effects exist to varying degrees in real materials and contribute to the emergent interface phenomena. However, whether and how these effects are physically connected, and what are their relative contributions, remain uncertain. Particularly, for defects, it is unclear which specific defects can be induced and are responsible for the emergent interface phenomena. Using first principles electronic and defect calculations, we identify the specific defects that can form spontaneously as a response to the built-in polar field and show how these defects lead to a unifying mechanism (**Figure 1**) that simultaneously explains the main features of both conductivity and magnetism at the interface.

The key physical quantities that feature in our explanation are (i) the formation energy ΔH (which controls the defect concentration) (**Figure 2**) of the defect in various charge states at thermodynamic equilibrium Fermi-energy E_F , and (ii) the donor or acceptor electrical levels (**Figure 3**), i.e., the defect charge transition energy $\varepsilon(q/q')$ defined as the E_F where the ΔH of a defect at two different charge states q and q' equal. A donor can produce electrons and compensate holes, whereas an acceptor can produce holes and compensate electrons. These two quantities (i) and (ii) have not been previously calculated for charged defects in different layers across the interfaces and turn out to be crucial. The details of their first principles calculations are given in Methods section.

The central point of the proposed mechanism is that the polar-discontinuity induced built-in polar field triggers thermodynamically the spontaneous formation of the certain defects at surface and/or interface, which in turn compensate the built-in polar field and thus avoids the potential divergence. Thus, it is the polar-field induced defects, rather than the electronic or atomic reconstruction, that are responsible for the conductivity and magnetism at the interface. Specifically, we find that the surface donor defect (here V_O) has its donor levels located energetically above the SrTiO_3 conduction band at the interface but below the LaAlO_3 conduction band. This donor level position is a prerequisite for 2DEG formation. Although the 2DEG owes its *existence* to the surface donors, the *density* of 2DEG is controlled by the interfacial deep acceptor defects (mainly Al-on-Ti antisite). It is also turn out that the interface magnetic moment is caused by the unionized deep Ti-on-Al antisite defects located within the LaAlO_3 side near the interface.

In what follows we address specifically how this polar-field induced defect mechanism resolves the long-standing puzzles on the origin of 2DEG, the critical thickness for 2DEG, the weak field in LaAlO_3 film, the density of 2DEG, the insulating p-type interfaces, and the origin of the local magnetism moments. During this process, we also distill the general rules that control the pertinent effects and allow future section of other polar-nonpolar interface materials with similar or improved interface properties.

1. What creates the 2DEG?

The 2DEG is unlikely to originate from the defect-free scenarios: these include the ionization of the intrinsic LaAlO₃ valence bands (suggested by the polar catastrophe model^{3,4}) or the ionization of the LaO interface layer (suggested by the interfacial charge leaking model)³⁶ (Supplementary note 1). This is simply because that the creation of 2DEG in these defect-free scenarios requires the LaAlO₃ valence band maximum (VBM) to cross the SrTiO₃ conduction band minimum (CBM) or Fermi-energy E_F . This is contrary to the experimentally observed weak field (negligible band-bending)³⁷⁻⁴⁰ in the LaAlO₃ film, clearly showing that the LaAlO₃ VBM is far below the E_F .

The 2DEG also is unlikely to originate from interfacial point donor defects (La_{Sr}, Ti_{Al}, and V_O). Recall first that the defect formation energy ΔH depends on the E_F (or chemical potential) and the defect charge transition energy $\varepsilon(q/q')$ needs to be close to band edges in order to producing free carriers. In thermodynamic equilibrium, the E_F of the system pins around the middle of SrTiO₃ band gap when $n_{LAO} < L_c$, and around the SrTiO₃ conduction band edge near the interface when $n_{LAO} \geq L_c$ (Supplementary note 2). In either case, Fig.2ab shows that the ΔH of the anti-site donor defects, La_{Sr}⁰ and Ti_{Al}⁰ is small positive or even negative (note: the superscript denotes the *defect charge states*, not the nominal *oxidation state* of the atom at the defect site). In other words, the formation of such antisite defects at the thermodynamic equilibrium E_F is energetically favorable and would inevitably lead to interfacial cation mixing. However, at such E_F , both La_{Sr}⁰ and Ti_{Al}⁰ defects are stable in their charge *neutral* states (as indicated by the superscript), contributing no free carriers. On the other hand, the interfacial V_O defects are energetically stable in the charged states, i.e., V_O²⁺ (Fig.2ab). This means that if formed, the V_O will donate electrons and thereby become positively charged. However, the ΔH of V_O²⁺ at such equilibrium E_F is rather high ($> 2.5\text{eV}$), implying that V_O²⁺ have very low concentration under thermodynamic equilibrium conditions. The high ΔH also means that even if the V_O defects are formed under non-equilibrium growth conditions, they can still be removed easily by the post O-rich annealing process⁴¹ (Supplementary note 3). Thus, contrary to earlier postulations, these interfacial donor defects are not responsible for 2DEG, consistent with recent experiments⁴².

The oxygen vacancy, V_O(S), at the free LaAlO₃ surface can explain the interfacial 2DEG. For this to happen, three conditions (“design principles”) need to be satisfied. First, V_O(S) in the polar film material needs to have a sufficiently low formation energy ΔH so it could form. Fig.4a shows the ΔH of V_O(S) decreases linearly as the film thickness n_{LAO} increases, consistent with previous calculations^{20,43}. When $n_{LAO} \geq 3-4$ uc, the ΔH becomes zero or negative, and V_O(S) will form spontaneously and be stable even for high oxygen chemical potentials. (This suggests that even exposing the surface to air or post-annealing under O-rich environment cannot heal these vacancies). Second, the donor transition level of V_O(S) in the polar film material should be higher in energy than the substrate (SrTiO₃) conduction band edge at the interface. Fig.3 shows that this condition is also satisfied. Third, the system needs to have a non-zero built-in polar field that would enable the electron to transfer from the surface to the interface. Such transfer sets up an opposite dipole (proportional to n_{LAO}), which in turn cancels the field and lowers the ΔH . The larger the n_{LAO} , the lower the ΔH . Note that in the absence of such field, the surface-to-interface charge transfer would not occur since such a transfer would create a dipole that would increase the electrostatic energy (proportional to that dipole) and thus raise the total energy of the system. These three conditions are satisfied in this LaAlO₃/SrTiO₃ system.

It is important to note that the built-in polar field always exists during the layer-by-layer growth. This is because that the surface defects (here V_O) can cancel the built-in polar field only

in the LaAlO₃ film between the interface and the surface, not the built-in polar field in the LaAlO₃ film to be grown on top of the surface. Such polar field can then always trigger V_O formation at the surface of LaAlO₃ film to be grown, no matter whether the polar field has been cancelled in the LaAlO₃ substrate or not.

The emerging picture for the formation of the 2DEG is that the electrons ionized from V_O(S) of the polar film material transfer to the nonpolar substrate material SrTiO₃ conduction bands at the interface via the built-in polar field, thus forming the 2DEG at that interface. This charge transfer in turn cancels the built-in polar field in LaAlO₃. After the built-in field has been cancelled, the ΔH of V_O(S) return to a high value (> 3 eV) characteristic of the bulk, and V_O(S) become again hard to form in thermodynamic equilibrium²⁰. Thus, the maximum concentration of V_O(S) is $0.25/S_{2D}$ (where S_{2D} is 2D unit cell area), i.e., one of eight oxygen missing at surface, donating $0.5 e/S_{2D}$ that cancels the polar field in LaAlO₃ completely. The compensation of polar field by V_O(S) also means that the band bending in LaAlO₃ due to polar field is also removed. Thus, the LaAlO₃ valence bands fall well below the E_F , contrary to what the polar catastrophe model would suggest. Consequently, no free holes can arise from depopulation of the LaAlO₃ valence bands at the surface, consistent with experiments^{3,22}.

The emerging design principles for selecting materials that will likely form interface 2DEG: (i) the nonpolar material has a conduction band minimum (CBM) sitting in the band gap of the polar material; (ii) The polar material has at least one *deep* donor defect with its donor level higher than the conduction band of the nonpolar material at the interface. The (i) and (ii) in together guarantee that the 2DEG forms only at the n-type interfaces. This picture suggests that the 2DEG at n-type LaAlO₃/SrTiO₃ interfaces may also be induced and/or tuned by using some surface adsorbates (e.g., H₂O, H)⁴⁴⁻⁴⁶ or metallic contacts⁴⁷ provided that the ionization energy of the surface adsorbate or the metallic contact is not lower than the donor level of the V_O(S).

2. What controls the critical thickness?

The linear decrease of ΔH of V_O(S) with increasing polar film thickness n_{LAO} naturally explains the critical thickness L_c for the metal-insulator transition. The rate of decrease (i.e., the slope $d\Delta H/dn_{LAO}$) equals 0.19 eV/Å, which is same as the calculated built-in polar field in the defect-free LaAlO₃ film (Supplementary note 4). The V_O(S) defects start to form spontaneously when the ΔH becomes zero at an L_c of ~ 4 uc under a typical O-rich growth condition (Fig.3a). For the LaAlO₃ film that is one unit cell thinner than this L_c , the calculated ΔH of V_O(S) is 0.75 eV, which is too high to produce significant free carrier concentration. Thus, *the appearance of V_O(S) (and the ensuing metal-insulator transition) at L_c is predicted to be sharp, distinct from the gradual appearance of 2DEG behavior as predicted from polar catastrophe model, but consistent with experiments*⁴⁸.

Fig.3a suggests that the L_c resulting from V_O(S) is controlled by the formation energy ΔH_o of V_O at interface (or the ΔH extrapolated at $n_{LAO} = 0$) and the polar field E_p via $L_c = \Delta H_o/eE_p$. Since $E_p = 4\pi P_0/\epsilon$ (where ϵ and P_0 are the dielectric constant and formal polarization of LaAlO₃ film), this relation can be written as $L_c = \Delta H_o\epsilon/4\pi eP_0$, which predicts an L_c of ~ 4 uc, depending slightly on the O-poor/rich growth conditions (Supplementary note 5). The relation of $L_c = \Delta H_o\epsilon/4\pi eP_0$ provides an alternative explanation for the observed variation of the L_c with the fraction x in (LaAlO₃)_{1-x}(SrTiO₃)_x overlayer (where P_0 is proportional to x)⁴⁹. This observation was originally explained by $L_c = \Delta\Phi\epsilon/4\pi eP_0$ (where $\Delta\Phi$ is the energy difference between LaAlO₃ VBM and SrTiO₃ CBM) within polar catastrophe model⁴⁹. Since $\Delta\Phi$ and ΔH_o have

similar value ($\sim 3-4$ eV), it is not surprising that the L_c predicted from these two models is also similar.

Implication on the design of carrier mobility: (i) The relatively high 2DEG mobility may be enabled by a modulated doping effect⁵⁰, whereby the source of carriers (here at the LaAlO₃ surface) is spatially separated from the place where the carriers reside (here at the LaAlO₃/SrTiO₃ interface), thus minimizing carrier scattering by the defects. This minimal spatial separation is measured by the critical thickness L_c . The relationship $L_c = \Delta H_o \epsilon / 4\pi e P_0$ suggests that a large L_c (hence maintaining *good mobility*) *could be achieved by selecting a polar materials with small polarization, large dielectric constant, and donor defects characterized by high formation energy ΔH at the interface or in the bulk.* On the other hand, (ii) the concentration of interfacial defects should be minimized in order to take advantage of (i). In addition, (iii) since the 2DEG is located at the conduction bands of the nonpolar material, it is advantageous to select the nonpolar material with low electron effective mass in order to achieve higher mobility.

3. What compensates the built-in polar field?

Experimentally, only very weak residual field has been observed in the LaAlO₃ film no matter whether its thickness is below or above the L_c ³⁷⁻⁴⁰. This observation cannot be explained within the defect-free interface scenario. In turn, whereas the $V_O(S)$ model explains the weak electric field in LaAlO₃ film *above* the L_c , it does not explain it *below* the L_c . This leads us to inspect the effects of all possible cation antisite defects across the interface.

In term of point defect, each interfacial antisite alone cannot cancel the polar field. Fig.2ab shows that the La_{Sr}, Sr_{La}, Ti_{Al}, and Al_{Ti} antisite defects have lower ΔH than other point defects (e.g., vacancy) in the layer where they are located. This means that these four antisite defects are the dominating defects in their corresponding layers. Apparently, the interfacial La_{Sr} donor in SrTiO₃ side cannot set up an opposite dipole across the LaAlO₃ film that can cancel the polar field inside the LaAlO₃ film. For the Ti_{Al} donor in LaAlO₃ side, since its donor level is lower than the SrTiO₃ conduction band at the interface, the ionized electrons cannot be transferred to the latter either to cancel the polar field. For interfacial Al_{Ti} and Sr_{La} acceptors, the polar field compensation is similar to that in polar catastrophe model: before the LaAlO₃ VBM reaches the acceptor levels of Al_{Ti} or Sr_{La}, the polar field cannot be cancelled; After that, the electrons start to transfer from LaAlO₃ valence bands to the acceptor levels of these defects, and the internal field decreases gradually as n_{LAO} increase, approaching zero at infinitely large n_{LAO} .

The [Ti_{Al}+Al_{Ti}] defect pair is the most potent source of polar field cancellation among those donor-acceptor antisite defect pairs at n-type interfaces. The four leading antisite defects can form four types of donor-acceptor pairs: [Ti_{Al}+Al_{Ti}], [La_{Sr}+Sr_{La}], [La_{Sr}+Al_{Ti}], and [Ti_{Al}+Sr_{La}], which are denoted as ①, ②, ③, ④ respectively in Fig.3. Clearly, the electron-transfer from donor to acceptor in both pair ② and ③ is unlikely since it will create a dipole in the *same direction* as the intrinsic dipole in LaAlO₃, and thus *increase* the dipole moment (also the electrostatic energy) and destabilize the interface. In both pair ① and ④, the charge transfer can cancel the polar field. However, the electron transfer in pair ① is energetically much more favorable because (i) Al_{Ti} has a lower acceptor level than Sr_{La} and (ii) the donor-acceptor separation distance (also the associated opposite dipole moment that lowers the total energy of the system) is larger in pair ① (Fig.3a).

For $n_{LAO} < L_c$, the [Al_{Ti}+Ti_{Al}] can form spontaneously via Ti \leftrightarrow Al exchange across the interface and cancel the polar field. Fig.4b (filled symbols) shows that the energy required to

form such defect pair is negative (i.e., exothermic), and the largest energy gain is obtained when a Ti atom of TiO₂-interface monolayer is exchanged with an Al of AlO₂-surface monolayer, i.e., Al_{Ti}(I)+Ti_{Al}(S), which is consistent with previous first-principles calculations⁵¹. This means that Ti atom at the interface would hop to the AlO₂ surface layer and exchange with Al atom there. Similar to that of V_O(S), the linear decrease of ΔH with increasing donor-acceptor separating distance (Fig.4b) is a sign of polar field compensation by electron transfer from Ti_{Al} donor to Al_{Ti} acceptor, which is expected since the donor level is higher than acceptor level (Fig.3a). Fig.4a also shows that the V_O(S) has too high ΔH to form for $n_{LAO} < L_c$ (Fig.4a). Therefore, the polar field is cancelled by those spontaneously formed [Al_{Ti}(I)+Ti_{Al}(S)] pairs. On the other hand, since these defects are deep, they cannot cause free carriers in the both interface and surface regions (whence insulating).

For $n_{LAO} \geq L_c$, the polar field is cancelled by spontaneously formed V_O(S), not by [Al_{Ti}(I)+Ti_{Al}(S)]. Recall that the polar field always exists in the LaAlO₃ layers during the lay-by-layer growth. The existence of this polar field can always trigger the formation of V_O(S) and/or Ti_{Al}(S) defects as n_{LAO} increases. For $n_{LAO} \geq L_c$, both V_O(S) (Fig.4a) and [Al_{Ti}(I)+Ti_{Al}(S)] pair (Fig.4b) have zero or negative ΔH , meaning that both could form in ideal interfaces. However, if both V_O(S) and Ti_{Al}(S) present, since V_O has a higher donor level than Ti_{Al} (Fig.3a), the electron transfer from V_O(S) to Al_{Ti}(I) is energetically more favorable than that from Ti_{Al}(S) to Al_{Ti}(I), and the polar field is thus always cancelled by the former. After the polar field has been cancelled by V_O(S), Fig.4b (open symbols) shows that the ΔH of [Al_{Ti}(I)+Ti_{Al}(S)] pair becomes positive (0.4-0.7 eV), meaning that [Ti_{Al}+Al_{Ti}] pairs cannot be formed via Ti \rightleftharpoons Al exchange over a distance beyond L_c . Therefore, for $n_{LAO} \geq L_c$, only V_O(S) defects can form and cancel the polar field.

4. What controls the density of 2DEG?

Reinterpretation of the puzzle: According to Gauss' law, the experimentally observed weak electric field in LaAlO₃ film means that the total external charge density (mobile and/or immobile) at the interface must be $\sim 0.5 e/S_{2D}$ (Supplementary note 6). For $n_{LAO} < L_c$, not conductivity at interfaces means that all (or almost all) interfacial charge does not contribute to the conductivity. For $n_{LAO} \geq L_c$, only a fraction of $0.5 e/S_{2D}$ interfacial charge is seen in transport and so the majority of $0.5 e/S_{2D}$ charge does not contribute to the conductivity. The puzzle thus is why the $\sim 0.5 e/S_{2D}$ charge exists at the interface with any n_{LAO} but only a small part of it contribute to conducting 2DEG when $n_{LAO} \geq L_c$. This puzzle cannot be explained within defect-free interface scenario by polar catastrophe model^{3,4} or interfacial charge leaking model³⁶, since both predict zero interfacial charge for $n_{LAO} < L_c$ and an interfacial charge density much higher than the measured 2DEG density for $n_{LAO} \geq L_c$ (Supplementary Fig.S1). The possibility of multiple carrier types (i.e., the electrons occupying d_{xy} and those occupying d_{xz}/d_{yz} sub-bands contribute differently in transport) at ideal interfaces has also been suggested to explain the measured 2DEG density above the L_c ⁵²⁻⁵⁵. Similarly, the existence of such multiple carrier types could not explain the $0.5 e/S_{2D}$ interface charge that indeed exists. Moreover, it is also difficult to reconcile why a full carrier density of $0.5 e/S_{2D}$ has been observed at GdTlO₃/SrTiO₃ interfaces (where the same multiple carrier types exist)⁵⁶.

The 2DEG density is controlled by the concentration of immobile acceptor defects that can trap itinerant electrons. Within the emerging defect picture, the total interfacial charge is always $\sim 0.5 e/S_{2D}$, which corresponds to the (almost) complete polar field cancellation. In SrTiO₃ side (where the 2DEG is located), there are mainly three types of acceptor defects, namely, Al_{Ti}, V_{Sr}, and V_{Ti}. At equilibrium E_F , Fig.2ab shows that these acceptor defects all

prefer to stay in negative charge states, i.e., $\text{Al}_{\text{Ti}}^{1-}$, $\text{V}_{\text{Sr}}^{2-}$, and $\text{V}_{\text{Ti}}^{4-}$. (In other defect charge states, these defects have much higher ΔH and are not shown in Fig.2ab). It means that once these defects form they will trap free electrons from the system and get negatively charged. Among these acceptor defects, $\text{Al}_{\text{Ti}}^{1-}$ acceptors have the lowest ΔH and thus they are the most potent electron-trapper. For $n_{\text{LAO}} < L_c$, the Al_{Ti} defects resulting from $\text{Ti} \leftrightarrow \text{Al}$ exchange trap all free electrons transferred from $\text{Ti}_{\text{Al}}(\text{S})$ defects, and hence no free carrier can occur. For $n_{\text{LAO}} \geq L_c$, due to $\text{V}_{\text{O}}(\text{S})$, the ΔH of $[\text{Ti}_{\text{Al}} + \text{Al}_{\text{Ti}}]$ pair changes from negative to positive (Fig.4b), meaning that the concentration of Al_{Ti} defect resulting from $\text{Ti} \leftrightarrow \text{Al}$ exchange is reduced, compare to that formed below the L_c . Therefore, the Al_{Ti} defect concentration is not sufficient to trap all $0.5e/S_{2D}$ electrons transferred from $\text{V}_{\text{O}}(\text{S})$. Therefore, only a small fraction of $0.5 e/S_{2D}$ can contribute to interface 2DEG.

The recently observed LaAlO₃ cation-stoichiometry effect on 2DEG formation⁴² may also be understood within above picture. For Al-rich LaAlO₃ film, where both A-site and B-site sublattices are fully occupied (hence having no cation vacancies), the Al_{Ti} anti-sites are the only electron-trapping defects and the incomplete trapping of $0.5e/S_{2D}$ interface charge by Al_{Ti} defects leads to interface conductivity. However, for La-rich LaAlO₃ film, where B-site sublattice is not fully occupied, the cation vacancies (V_{Ti} and V_{Al}) also become main electron-trappers, in addition to $\text{Al}_{\text{Ti}}(\text{I})$. Though, the concentration of Al_{Ti} is reduced, each cation vacancy induced in La-rich film traps more electrons than an Al_{Ti} . The insulating character can be then attributed to the complete interfacial electron trapping by both interfacial cation vacancies and $\text{Al}_{\text{Ti}}(\text{I})$.

The picture of $\text{Al}_{\text{Ti}}(\text{I})$ as main electron-trapping defects may be extended to SrTiO₃/GdTiO₃ interfaces. The observed full carrier density of $0.5 e/S_{2D}$ there⁵⁶ can be ascribed to the fact that both SrTiO₃ and GdTiO₃ have the same Ti atom at B-site sublattice and have no Al_{Ti} -like antisite defects at the interface.

Implication on how to increase the density of 2DEG: The above picture suggests that the main controlling factor for the interface carrier density is the concentration of the acceptor defects (mainly Al_{Ti} in stoichiometric or Al-rich film), which should be minimized for enhancing carrier density. Such Al_{Ti} -like electron trapping defects may be completely removed by designing other oxide interfaces like GdTiO₃/SrTiO₃ interfaces, whose bulk components have a common cation atom with multiple valence states.

5. Why are the p-type interfaces insulating?

The intriguing fact is that the so-called p-type interfaces are not p-type (hole) conducting and are actually insulating. The defect-free polar-catastrophe model for p-type interface predicts a hole conducting interface and an electron conducting surface when $n_{\text{LAO}} > \sim 7.3$ uc (Supplementary Fig.1) in contradiction with the insulating behavior observed robustly in experiment. To explain this, defects thus be involved. The emerging defect picture below differs from the literature model based solely on interfacial hole-polaron⁵⁷ or interfacial hole-compensating V_{O} defects^{23,43}, which assumes that the interface has holes arising from the depopulation of the intrinsic SrTiO₃ valence bands.

Interfacial point defects can neither cause conductivity nor cancel the polar field. Similar to that at n-type interfaces, the interfacial La_{Sr} and Ti_{Al} are stable at their charge neutral states and have negligible or negative ΔH at equilibrium E_F . It means that they cause inevitable interfacial cation intermixing but induce no free carriers. The V_{O} and other defects at the interface have too high ΔH to form and thus they do not produce free carriers either. Also for similar reason,

each leading antisite defect (La_{Sr} , Sr_{La} , Ti_{Al} , or Al_{Ti}) alone at p-type interfaces cannot cancel the polar field.

The spontaneously formed donor-acceptor defect pairs always cancel the polar field but do not induce free carriers. In the p-type interfaces, the polar field points from surface to interface, which is opposite to that in the n-type interfaces. Among four donor-acceptor defect pairs as indicated in Fig.3b, the pair $\textcircled{2}$ (i.e., $[\text{La}_{\text{Sr}}+\text{Sr}_{\text{La}}]$) is energetically most favorable in polar field cancellation. For $n_{\text{LAO}} < \sim 4\text{uc}$, the $[\text{La}_{\text{Sr}}(I)+\text{Sr}_{\text{La}}(S)]$ pairs have negative ΔH (Fig.4d) and can form spontaneously via $\text{La} \Leftrightarrow \text{Sr}$ exchanges, whereas the $[\text{La}_{\text{Sr}}(I)+\text{V}_{\text{La}}(S)]$ have too high ΔH to form (Fig.4c). So the polar field is cancelled by the charge transfer from $\text{La}_{\text{Sr}}(I)$ to $\text{Sr}_{\text{La}}(S)$, which can be expected from their relative defect levels (Fig. 3b) and their linear decreasing behavior in ΔH as a function of n_{LAO} (Fig.4d). For $n_{\text{LAO}} \geq \sim 4\text{uc}$, the ΔH of $[\text{La}_{\text{Sr}}(I)+\text{V}_{\text{La}}(S)]$ become negative (Fig.4c) and can also form spontaneously. Since V_{La} has a lower acceptor level than Sr_{La} (Fig.3b), the polar field is cancelled by the charge transfer from $\text{La}_{\text{Sr}}(I)$ to $\text{V}_{\text{La}}(S)$, rather than to $\text{Sr}_{\text{La}}(S)$. In absence of electric field, Fig.4d (open symbols) indicates that the $\text{La} \Leftrightarrow \text{Sr}$ exchanges cannot occur anymore over a distance of $\sim 4\text{uc}$. Unlike that in n-type interfaces, the $\text{V}_{\text{O}}(S)$ defects in p-type interface always have too high ΔH to form. The defects involved in polar field cancellation are all deep. The calculated equilibrium E_F according to those point defects turns out to stay always around the middle of SrTiO_3 band gap. It means that both VBM and CBM are far away from the E_F and there are no free carrier arising from the depopulation of VBM and CBM in both interface and surface regions (whence insulating).

Implication on the design of two-dimensional hole conductivity: Clearly, the formation of interfacial free holes is prevented by these spontaneously formed deep La_{Sr} defects that have donor level higher than the VBM at the interface. So to induce interfacial hole conductivity, one should search for the polar-nonpolar interfaces where all such donors have too high enough formation energy to form or (ii) their donor levels below the VBM at the interface. Practically, the (ii) may be achieved more easily by searching for the polar material whose VBM is higher than the charge transition energy levels of those spontaneously formed interfacial donor defects.

6. What causes interface magnetism?

Distinct from previous models³¹⁻³⁴ that explain magnetism based on interfacial $\text{Ti}(3+)$ *within the SrTiO_3* (i.e, not a defect), we find below that the local magnetic moment originates from the un-ionized deep Ti_{Al} anti site defect (i.e., $\text{Ti}(3+)$ -on- $\text{Al}(3+)$ *within LaAlO_3* side near the interface. The interface magnetism depends on the concentration and spatial distribution of such Ti_{Al} defects. This picture explains not only why the magnetism appears at n-type interfaces with a similar critical thickness to that for 2DEG, but also why the magnetism also appears at insulating p-type interfaces⁸.

What causes local moment: For n-type interfaces, when $n_{\text{LAO}} < L_c$, the polar field in LaAlO_3 is cancelled by the charge transfer from $\text{Ti}_{\text{Al}}(S)$ defects to the interface. These formed Ti_{Al} defects are thus ionized, i.e., $\text{Ti}_{\text{Al}}^{1+}$ (where superscript denotes the defect charge states). The Ti atom at this defect site has oxidation states of $4+$, denoted as, $\text{Ti}(4+)$ which has no local magnetic moment. When $n_{\text{LAO}} \geq L_c$, the polar field in LaAlO_3 is cancelled by the charge transfer to the interface from $\text{V}_{\text{O}}(S)$ instead of Ti_{Al} . All $\text{Ti}_{\text{Al}}(I)$ defects in LaAlO_3 film in absence of internal field are most stable in their charge neutral (or un-ionized) states, i.e., Ti_{Al}^0 , where Ti appears as $\text{Ti}(3+)$ oxidation state, having a finite local magnetic moment. Therefore, the interface magnetism at n-type interfaces due to those un-ionized Ti_{Al}^0 defects should also have a critical thickness of $\sim 4\text{uc}$. For p-type interfaces, it is the charge transfer among the defects other than

Ti_{Al} defects that cancels the polar field in in LaAlO₃. So all formed Ti_{Al} defects there are not ionized, having local magnetic moments, and can cause interface magnetism.

The magnitude of local moment: The local moment of a single Ti_{Al} defect at the interface can be estimated from that in bulk LaAlO₃, which is $0.84\mu_B$ from our hybrid functional calculation. For ferromagnetic order as observed in experiment, the total interface magnetic moment depends on the concentration of un-ionized Ti_{Al} defects in LaAlO₃ and can be very small per Ti atom in average. The experimentally observed inhomogeneous landscape of magnetism that also varies from sample to sample^{8,9} may be attributed to the various spatial distributions of Ti_{Al} defects, which may be sensitive to sample preparation conditions (such as temperature and P_{O_2}) and local strain.

Comparing with $V_O(I)$ model: Relative to $V_O(I)$ as the origin of local moment, the Ti_{Al}(I) defects within LaAlO side are more reasonable in at least two aspects. First, the deep Ti_{Al} defect is spatially localized and has an unambiguous local moment. While for V_O , which is a shallow donor, it donates electrons to the lower-energy interfacial Ti d_{xy} sub-bands that have light effective mass inside the interface plane⁵⁵, and the resulting Ti(3+) may then be itinerant. Second, the Ti_{Al} defects would form easily or even inevitable due to its small or negative ΔH , whereas the interfacial V_O require significant energy to form and if formed they may be removed completely after annealing.

Discussion

This work establishes a physical link between polar discontinuity and defect formation: the polar discontinuity triggers spontaneous formation of certain defects that in turn cancel the polar field induced by polar discontinuity. This link reveals a unifying mechanism that simultaneously explains the experimental observations listed in Table 1. This mechanism leads to a set of design rules for both conductivity and magnetism at the LaAlO₃/SrTiO₃ interfaces and enables the design of other polar-nonpolar interfaces (not limited to oxides) with similar or improved interface properties by first principles defect calculations.

Having ruled out the electronic reconstruction, interfacial V_O , and interfacial cation intermixing mechanism as the possible origin of 2DEG in our calculations, we conclude that the 2DEG at n-type interfaces with $n_{LAO} \geq L_c$ originates from the spontaneously formed $V_O(S)$ defects. This conclusion stems from the finding that the donor level of deep V_O in in LaAlO₃ side is higher than the SrTiO₃ conduction band edge at the interface. This finding explains why the formation energy of $V_O(S)$ decreases linearly as n_{LAO} increases. The linear decreasing relation reveals a general formula and some new controlling parameters for the critical thickness of sharp metal-insulator transition in absence of the electric field in the polar LaAlO₃ film.

Instead of causing 2DEG, we find that the defects resulting from interfacial cation anti sites play key roles in other aspects. Specifically, (i) the cation intermixing cancels the polar field only below the critical thickness for both-type of interfaces. (ii) the interfacial Al_{Ti} acceptor defects control the density of 2DEG. (iii) the un-ionized interfacial Ti_{Al} defects within LaAlO₃ side cause the local magnetic moments. The (iii) suggests that all previous models on interface magnetism based on Ti(3+) ions in SrTiO₃ side should be revisited. Importantly, we find that the cation mixing is confined near the interface and does not extend in LaAlO₃ side over more than ~ 4 uc, above which the cation intermixing is prevented by spontaneous formation of some surface vacancy defects. This spatial confinement is critical for realizing nanoscale interface magnetism.

This mechanism provides three distinctive predictions to be tested in experiment as further validation. (i) For n-type interfaces, the AlO₂-surface layer is dominated by Ti_{Al} defects when $n_{LAO} < L_c$ and by V_O defect when $n_{LAO} \geq L_c$. (ii) For p-type interfaces, the LaO-surface layer is dominated by Sr_{La} and V_{La} defects, respectively, below and above an L_c of ~ 4 uc. (iii) Ti⁴⁺ and Ti³⁺ signals exist in both sides of the interface. The appearance of the Ti³⁺ signals should not be taken as a sign of conductivity. Whether the Ti³⁺ signals detected by photoemission below the L_c ^{21,39,58,59} can be truly assigned to those Ti³⁺ ions in SrTiO₃ side should be revisited carefully. How these Ti_{Al} local moments are ordered (ferromagnetic, or antiferromagnetic, or else) and whether and how they interact with the itinerant 2DEG are still open questions that should be investigated further.

Methods

All calculations were performed using density functional theory (DFT) and plane-wave projector augmented-wave (PAW)⁶⁰ method as implemented in the VASP code⁶¹. An energy cutoff of 400 eV was used. The Brillouin zone was sampled by $8 \times 8 \times 1$ and $4 \times 4 \times 1$ **k**-point mesh for 1×1 and 2×2 in-plane supercell respectively. The atomic forces were relaxed to be less than 0.03 eV/Å. The in-plane lattice constant was fixed to 3.943 Å (the relaxed lattice constant of SrTiO₃ by GGA⁶²). In slab calculations, the 4 uc (~ 16 Å) vacuum layer was used and the dipole correction was always applied to remove artificial dipole interactions⁶³. The results in Fig.2 and Fig.3 were obtained by using HSE hybrid functional⁶⁴ on the top of the GGA relaxed structures.

The formation energy of a defect (D) calculated from $\Delta H_D^q(E_F, \mu) = E_D^q - E_H + \sum_{\alpha} n_{\alpha} (\mu_{\alpha}^0 + \Delta\mu_{\alpha}) + q(E_v + E_F)$, where E_D^q and E_H are the total energies of a supercell with and without defect, respectively, and D being in charge state q . n_{α} is the number of atoms of specie α needed to create a defect. E_F is the Fermi energy relative to VBM (E_v). $\Delta\mu_{\alpha}$ is the relative chemical potential of specie α with respect to its elemental solid (gas) (μ^0). The equilibrium Fermi-energy was calculated self-consistently according to charge neutrality condition⁶⁵. The chemical potentials relative to their elemental solid (or gas) phase are taken as variables and are bounded by the values that maintain a stable host compound and avoid formation of other competing phases in thermodynamic equilibrium (Supplementary Fig.S2). The details of theory and calculations can be found in Ref.[66].

Acknowledgements

This work was supported by the US Department of Energy, Office of Basic Energy Sciences as part of an Energy Frontier Research Centers, under the award No. DE-AC36-08GO28308 to National Renewable Energy Laboratory (NREL). The computation was done by using capabilities of the NREL Computational Sciences Center supported by the U.S. DOE office of Energy Efficiency and Renewable Energy, under Contract No. DE-AC36-08GO28308.

Author Contributions

L.Y. carried out the calculations, analyzed the results and wrote the paper. A.Z. initiated this study and contributed to the analysis of the results and the writing of the paper.

Table 1: List of the main puzzles and robust experimental observations at LaAlO₃/SrTiO₃ interfaces.

Interface structure	Experimental Observations	Polar Catastrophe	Cation Mixing	V ₀ at interface	V ₀ at surface	Current mechanism
n-type	1. Critical thickness (L_c) = 4 uc	✓	✗	✗	?	✓
	2. 2DEG density < 0.5 e/S	✗	?	✗	✗	✓
	3. Weak E in LaAlO ₃ for $n_{LAO} < L_c$	✗	?	✗	✗	✓
	4. Weak E in LaAlO ₃ for $n_{LAO} \geq L_c$	✗	✗	✗	✓	✓
	5. LaAlO ₃ surface: insulating	✗	?	?	✓	✓
	6. Interface: cation intermixed	✗	✓	✗	✗	✓
	7. Interface magnetism	✗	?	✗	✗	✓
p-type	1. Interface: insulating	✗	?	✗	?	✓
	2. LaAlO ₃ surface: insulating	✗	✗	?	?	✓
	3. Interface: cation mixed	✗	✓	✗	✗	✓
	4. Interface magnetism	✗	?	?	✗	✓

The symbol of ‘✓’ and ‘✗’ mean that the mechanism agrees or disagrees, respectively with the experimental observation. The ‘?’ symbol denotes uncertainty.

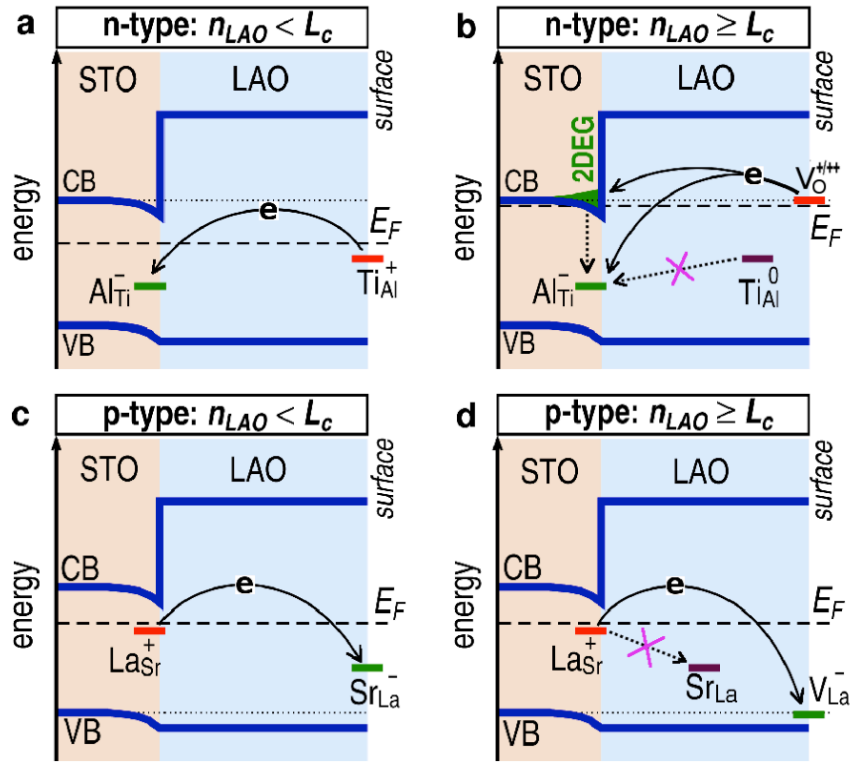


Figure 1: Schematic band and defect level picture for the unifying mechanism. **a**, n-type interfaces with $n_{LAO} < L_c$: The electrons transfer from $Ti_{Al}(S)$ to $Al_{Ti}(I)$ and compensate the electric field in $LaAlO_3$, inducing no itinerant carriers to the interface. **b**, n-type interfaces with $n_{LAO} \geq L_c$: The electrons transfer from $V_O(S)$ to interface. Part of interface charge is trapped by the deep Al_{Ti} acceptor defects. The deep Ti_{Al}^0 donor defects are confined within $LaAlO_3$ near the interface and are not ionized, i.e., Ti^{3+} -on- Al^{3+} , having local magnetic moments. **c**, p-type interfaces with $n_{LAO} < L_c$ ($\sim 4uc$): The electrons transfer from $La_{Sr}(I)$ to $Sr_{La}(S)$ and compensates the electric field in $LaAlO_3$. **d**, p-type interfaces with $n_{LAO} \geq L_c$: The electrons transfer from $La_{Sr}(I)$ to $V_{La}(S)$ and compensate the field in $LaAlO_3$. The superscripts (0,+,,+,-) denote the defect charge states, not the oxidation states of the ions there.

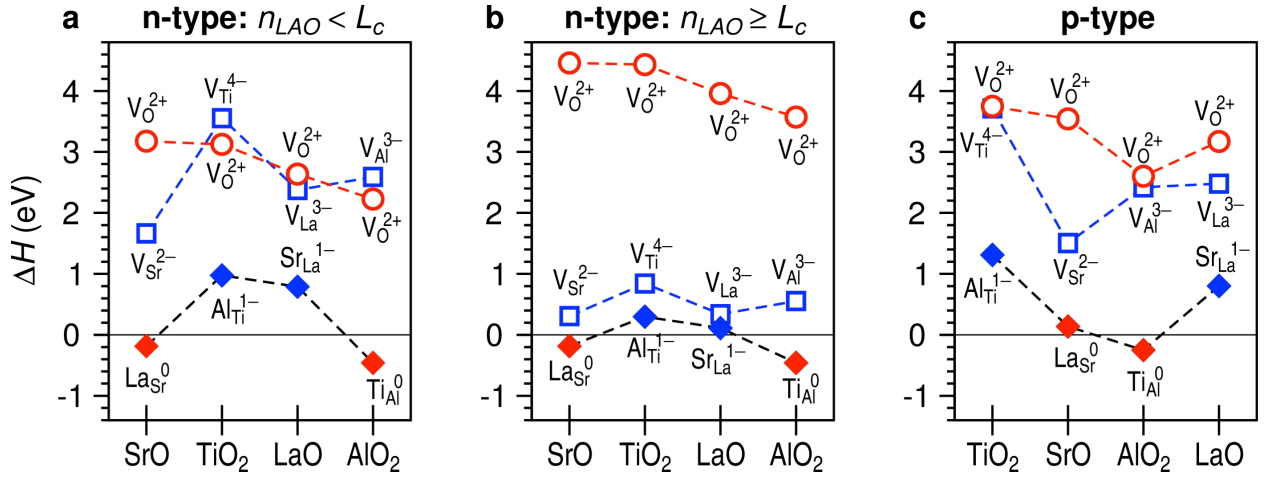


Figure 2: Formation energy of the interfacial point defects at thermodynamical equilibrium Fermi energy. **a,b**, n-type interfaces with $n_{LAO} < L_c$ and $n_{LAO} \geq L_c$, respectively. **c**, p-type interfaces. At a given E_F , the defect in different charge states (e.g., V_{Sr}^0 , V_{Sr}^{1-} , V_{Sr}^{2-}) usually has different ΔH and the only one with the lowest ΔH is shown in the Figure. Other cation defects that have higher ΔH are shown in Supplementary Fig. 3. The chemical potentials used for Sr, Ti, La, Al, and O are -4.36, -6.20, -6.10, -5.46, and -2.0 eV respectively, relative to their corresponding elemental solid or gas phases, which corresponds to $T=1050$ K and $P_{O_2} = 6.1 \times 10^{-6}$ Torr.

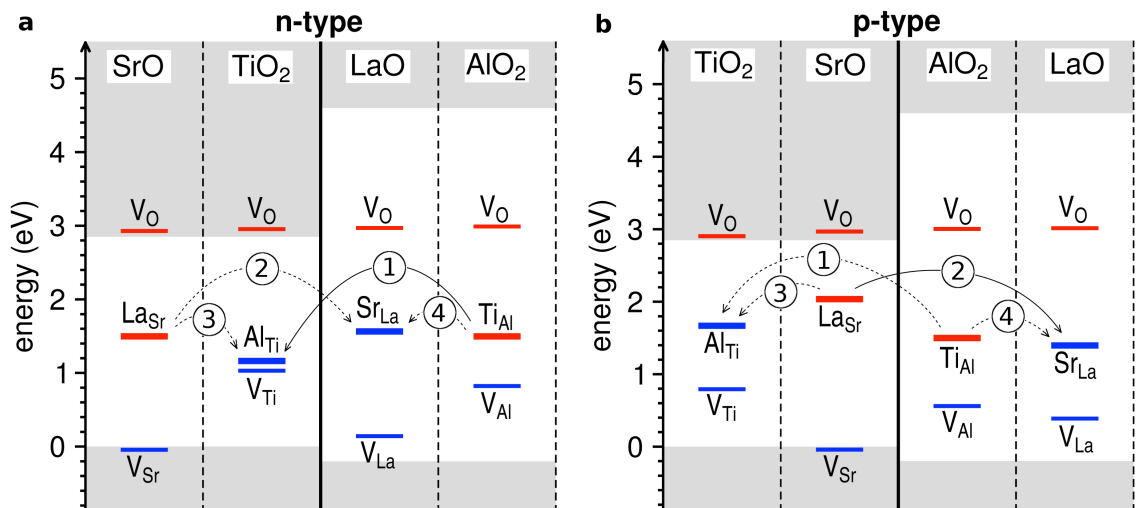


Figure 3: Defect charge transition energy levels of the interfacial point. a, n-type interface. **b,** p-type interface. The defect charge transition energy level is defined as the E_F where the ΔH of a given defect in two different charge states equal. Some defects may have multiple charge transition energy levels. For example, V_{Sr} has the two transition energy levels (one is for the transition between neutral charge state and -1, and the other is between -1 and -2). In such case, if the defect is donor (red), only the lowest level is shown, and if the defect is acceptor (blue), the highest level is shown.

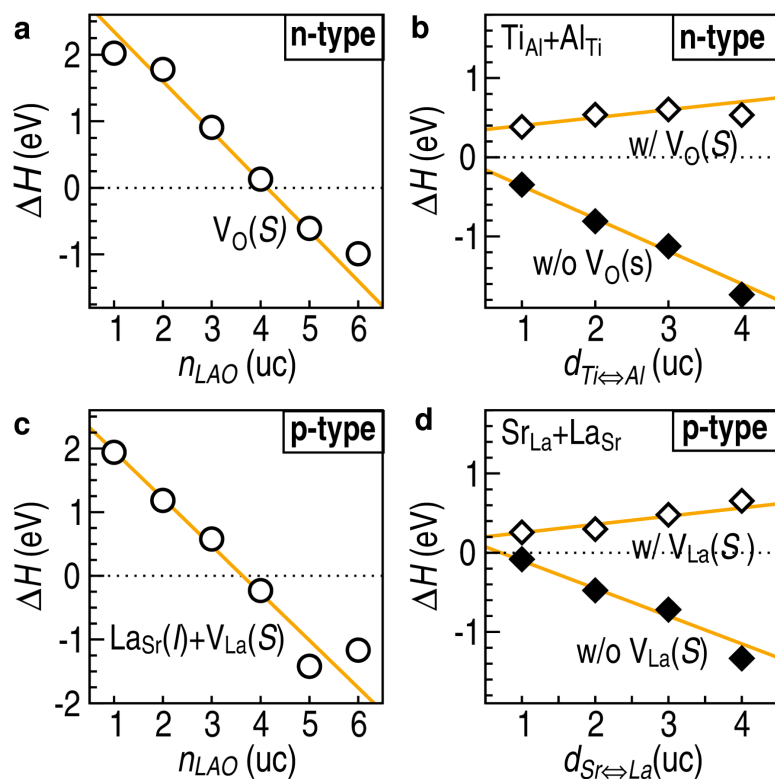


Figure 4: Properties of surface defects and defect complexes. **a**, the GGA-calculated ΔH of $V_O(S)$ defect, under the O-rich growth condition (i.e., $\Delta\mu_O = -1.5$ eV, Supplementary Fig. 2a). **b**, the ΔH of $[Ti_{Al}+Al_{Ti}]$ defect pair created from a $Ti \leftrightarrow Al$ exchange out of the ideal interface with and without a $V_O(S)$ in a 2×2 6STO/4LAO/vacuum supercell. **c**, the GGA-calculated ΔH of $[La_{Sr}(I)+V_{La}(S)]$ defect complex as a function of n_{LAO} , under $\Delta\mu_{Sr} = -4.36$ eV (Supplementary Fig. 1b). **d**, the ΔH of $[La_{Sr}+Sr_{La}]$ defect pair created from a $La \leftrightarrow Sr$ exchange out of the ideal interface with and without a $V_{La}(S)$ in a 2×2 6STO/4LAO/vacuum supercell, respectively. The $d_{Ti \leftrightarrow Al}$ and $d_{La \leftrightarrow Sr}$ in **b,d** are the distance between the components of corresponding defect pair. The orange lines are the guides to the eye.

References

- 1 Hwang, H. Y. *et al.* Emergent phenomena at oxide interfaces. *Nat Mater* **11**, 103-113 (2012).
- 2 Mannhart, J. & Schlom, D. G. Oxide Interfaces-An Opportunity for Electronics. *Science* **327**, 1607-1611 (2010).
- 3 Ohtomo, A. & Hwang, H. Y. A high-mobility electron gas at the LaAlO₃/SrTiO₃ heterointerface. *Nature* **427**, 423-426 (2004).
- 4 Thiel, S., Hammerl, G., Schmehl, A., Schneider, C. W. & Mannhart, J. Tunable quasi-two-dimensional electron gases in oxide heterostructures. *Science* **313**, 1942-1945 (2006).
- 5 Brinkman, A. *et al.* Magnetic effects at the interface between non-magnetic oxides. *Nat Mater* **6**, 493-496 (2007).
- 6 Li, L., Richter, C., Mannhart, J. & Ashoori, R. C. Coexistence of magnetic order and two-dimensional superconductivity at LaAlO₃/SrTiO₃ interfaces. *Nat Phys* **7**, 762-766 (2011).
- 7 Ariando *et al.* Electronic phase separation at the LaAlO₃/SrTiO₃ interface. *Nat Commun* **2**, 188 (2011).
- 8 Kalisky, B. *et al.* Critical thickness for ferromagnetism in LaAlO₃/SrTiO₃ heterostructures. *Nat Commun* **3**, 922 (2012).
- 9 Salman, Z. *et al.* Nature of Weak Magnetism in SrTiO₃/LaAlO₃ Multilayers. *Phys Rev Lett* **109**, 257207 (2012).
- 10 Lee, J. S. *et al.* Titanium d(xy) ferromagnetism at the LaAlO₃/SrTiO₃ interface. *Nat Mater* **12**, 703-706 (2013).
- 11 Joshua, A., Ruhman, J., Pecker, S., Altman, E. & Ilani, S. Gate-tunable polarized phase of two-dimensional electrons at the LaAlO₃/SrTiO₃ interface. *P Natl Acad Sci USA* **110**, 9633-9638 (2013).
- 12 Chen, H. H., Kolpak, A. M. & Ismail-Beigi, S. Electronic and Magnetic Properties of SrTiO₃/LaAlO₃ Interfaces from First Principles. *Adv Mater* **22**, 2881-2899 (2010).
- 13 Chakhalian, J., Millis, A. J. & Rondinelli, J. Whither the oxide interface. *Nat Mater* **11**, 92-94 (2012).
- 14 Siemons, W. *et al.* Origin of charge density at LaAlO₃ on SrTiO₃ heterointerfaces: Possibility of intrinsic doping. *Phys Rev Lett* **98**, 196802 (2007).
- 15 Kalabukhov, A. *et al.* Effect of oxygen vacancies in the SrTiO₃ substrate on the electrical properties of the LaAlO₃/SrTiO₃ interface. *Phys Rev B* **75**, 121404 (2007).
- 16 Herranz, G. *et al.* High mobility in LaAlO₃/SrTiO₃ heterostructures: Origin, dimensionality, and perspectives. *Phys Rev Lett* **98**, 216803 (2007).
- 17 Cen, C. *et al.* Nanoscale control of an interfacial metal-insulator transition at room temperature. *Nat Mater* **7**, 298-302, doi:Doi 10.1038/Nmat2136 (2008).
- 18 Zhong, Z. C., Xu, P. X. & Kelly, P. J. Polarity-induced oxygen vacancies at LaAlO₃/SrTiO₃ interfaces. *Phys Rev B* **82**, 165127 (2010).
- 19 Bristowe, N. C., Littlewood, P. B. & Artacho, E. Surface defects and conduction in polar oxide heterostructures. *Phys Rev B* **83**, 205405 (2011).
- 20 Li, Y., Phattalung, S. N., Limpijumnong, S., Kim, J. & Yu, J. Formation of oxygen vacancies and charge carriers induced in the n-type interface of a LaAlO₃ overlayer on SrTiO₃(001). *Phys Rev B* **84**, 245307 (2011).

- 21 Takizawa, M., Tsuda, S., Susaki, T., Hwang, H. Y. & Fujimori, A. Electronic charges and electric potential at LaAlO₃/SrTiO₃ interfaces studied by core-level photoemission spectroscopy. *Phys Rev B* **84**, 245124 (2011).
- 22 Berner, G. *et al.* Direct k-Space Mapping of the Electronic Structure in an Oxide-Oxide Interface. *Phys Rev Lett* **110**, 247601 (2013).
- 23 Nakagawa, N., Hwang, H. Y. & Muller, D. A. Why some interfaces cannot be sharp. *Nat Mater* **5**, 204-209, doi:Doi 10.1038/Nmat1569 (2006).
- 24 Willmott, P. R. *et al.* Structural basis for the conducting interface between LaAlO₃ and SrTiO₃. *Phys Rev Lett* **99**, 155502 (2007).
- 25 Kalabukhov, A. S. *et al.* Cationic Disorder and Phase Segregation in LaAlO₃/SrTiO₃ Heterointerfaces Evidenced by Medium-Energy Ion Spectroscopy. *Phys Rev Lett* **103**, 146101 (2009).
- 26 Yamamoto, R. *et al.* Structural Comparison of n-Type and p-Type LaAlO₃/SrTiO₃ Interfaces. *Phys Rev Lett* **107**, 036104 (2011).
- 27 Qiao, L., Droubay, T. C., Kaspar, T. C., Sushko, P. V. & Chambers, S. A. Cation mixing, band offsets and electric fields at LaAlO₃/SrTiO₃(001) heterojunctions with variable La:Al atom ratio. *Surf Sci* **605**, 1381-1387 (2011).
- 28 Vonk, V. *et al.* Polar-discontinuity-retaining A-site intermixing and vacancies at SrTiO₃/LaAlO₃ interfaces. *Phys Rev B* **85**, 045401 (2012).
- 29 Gunkel, F. *et al.* Influence of charge compensation mechanisms on the sheet electron density at conducting LaAlO₃/SrTiO₃-interfaces. *Appl Phys Lett* **100**, 052103 (2012).
- 30 Salluzzo, M. *et al.* Origin of Interface Magnetism in BiMnO₃/SrTiO₃ and LaAlO₃/SrTiO₃ Heterostructures. *Phys Rev Lett* **111**, 087204 (2013).
- 31 Banerjee, S., Erten, O. & Randeria, M. Ferromagnetic exchange, spin-orbit coupling and spiral magnetism at the LaAlO₃/SrTiO₃ interface. *Nat Phys* **9**, 625-629 (2013).
- 32 Fidkowski, L., Jiang, H. C., Lutchyn, R. M. & Nayak, C. Magnetic and superconducting ordering in one-dimensional nanostructures at the LaAlO₃/SrTiO₃ interface. *Phys Rev B* **87**, 014436 (2013).
- 33 Michaeli, K., Potter, A. C. & Lee, P. A. Superconducting and Ferromagnetic Phases in SrTiO₃/LaAlO₃ Oxide Interface Structures: Possibility of Finite Momentum Pairing. *Phys Rev Lett* **108**, 117003 (2012).
- 34 Pavlenko, N., Kopp, T., Tsymbal, E. Y., Mannhart, J. & Sawatzky, G. A. Oxygen vacancies at titanate interfaces: Two-dimensional magnetism and orbital reconstruction. *Phys Rev B* **86**, 064431 (2012).
- 35 Higuchi, T. & Hwang, H. Y. in *Multifunctional oxide heterostructures* (eds E. Y. Tsymbal, E. R. A. Dagotto, Chang-Beom Eom, & R. Ramesh) (Oxford University Press, 2012).
- 36 Janotti, A., Bjaalie, L., Gordon, L. & Van de Walle, C. G. Controlling the density of the two-dimensional electron gas at the SrTiO₃/LaAlO₃ interface. *Phys Rev B* **86**, 241108 (2012).
- 37 Segal, Y., Ngai, J. H., Reiner, J. W., Walker, F. J. & Ahn, C. H. X-ray photoemission studies of the metal-insulator transition in LaAlO₃/SrTiO₃ structures grown by molecular beam epitaxy. *Phys Rev B* **80**, 241107 (2009).
- 38 Huang, B. C. *et al.* Mapping Band Alignment across Complex Oxide Heterointerfaces. *Phys Rev Lett* **109**, 246807 (2012).

- 39 Slooten, E. *et al.* Hard x-ray photoemission and density functional theory study of the internal electric field in SrTiO₃/LaAlO₃ oxide heterostructures. *Phys Rev B* **87**, 085128 (2013).
- 40 Berner, G. *et al.* Band alignment in LaAlO₃/SrTiO₃ oxide heterostructures inferred from hard x-ray photoelectron spectroscopy. *Phys Rev B* **88**, 115111 (2013).
- 41 Van de Walle, C. G. & Neugebauer, J. First-principles calculations for defects and impurities: Applications to III-nitrides. *J Appl Phys* **95**, 3851-3879 (2004).
- 42 Warusawithana, M. P. R., C.; Mundy, J. A.; Roy, P.; Ludwig, J.; Paetel, S.; Heeg, T.; Pawlicki, A. A.; Kourkoutis, L. F.; Zheng, M.; Lee, M.; Mulcahy, B.; Zander, W.; Zhu, Y.; Schubert, J.; Eckstein, J. N.; Muller, D. A.; Hellberg, C. S.; Mannhart, J.; Schlom, D. G. LaAlO₃ stoichiometry is key to electron liquid formation at LaAlO₃/SrTiO₃ interfaces. *Nat Commun* **4**, 2351 (2013).
- 43 Zhang, L. X. *et al.* Origin of insulating behavior of the p-type LaAlO₃/SrTiO₃ interface: Polarization-induced asymmetric distribution of oxygen vacancies. *Phys Rev B* **82**, 125412 (2010).
- 44 Xie, Y. W., Hikita, Y., Bell, C. & Hwang, H. Y. Control of electronic conduction at an oxide heterointerface using surface polar adsorbates. *Nat Commun* **2**, 494 (2011).
- 45 Bi, F. *et al.* "Water-cycle" mechanism for writing and erasing nanostructures at the LaAlO₃/SrTiO₃ interface. *Appl Phys Lett* **97**, 173110 (2010).
- 46 Son, W. J., Cho, E., Lee, J. & Han, S. Hydrogen adsorption and carrier generation in LaAlO₃-SrTiO₃ heterointerfaces: a first-principles study. *J Phys-Condens Mat* **22**, 315501 (2010).
- 47 Arras, R., Ruiz, V. G., Pickett, W. E. & Pentcheva, R. Tuning the two-dimensional electron gas at the LaAlO₃/SrTiO₃(001) interface by metallic contacts. *Phys Rev B* **85**, 125404 (2012).
- 48 Liu, Z. Q. *et al.* Origin of the Two-Dimensional Electron Gas at LaAlO₃/SrTiO₃ Interfaces: The Role of Oxygen Vacancies and Electronic Reconstruction. *Phys Rev X* **3**, 021010 (2013).
- 49 Reinle-Schmitt, M. L. *et al.* Tunable conductivity threshold at polar oxide interfaces. *Nat Commun* **3**, 932 (2012).
- 50 Dingle, R., Stormer, H. L., Gossard, A. C. & Wiegmann, W. Electron Mobilities in Modulation-Doped Semiconductor Heterojunction Super-Lattices. *Appl Phys Lett* **33**, 665-667 (1978).
- 51 Chambers, S. A. *et al.* Instability, intermixing and electronic structure at the epitaxial LaAlO₃/SrTiO₃(001) heterojunction. *Surf Sci Rep* **65**, 317-352 (2010).
- 52 Popovic, Z. S., Satpathy, S. & Martin, R. M. Origin of the Two-Dimensional Electron Gas Carrier Density at the LaAlO₃ on SrTiO₃ Interface. *Phys Rev Lett* **101**, 256801 (2008).
- 53 Son, W. J., Cho, E., Lee, B., Lee, J. & Han, S. Density and spatial distribution of charge carriers in the intrinsic n-type LaAlO₃-SrTiO₃ interface. *Phys Rev B* **79**, 245411 (2009).
- 54 Seo, S. S. A. *et al.* Multiple conducting carriers generated in LaAlO₃/SrTiO₃ heterostructures. *Appl Phys Lett* **95**, 082107 (2009).
- 55 Delugas, P. *et al.* Spontaneous 2-Dimensional Carrier Confinement at the n-Type SrTiO₃/LaAlO₃ Interface. *Phys Rev Lett* **106**, 166807 (2011).
- 56 Moetakef, P. *et al.* Electrostatic carrier doping of GdTiO₃/SrTiO₃ interfaces. *Appl Phys Lett* **99**, 232116 (2011).

- 57 Pentcheva, R. & Pickett, W. E. Charge localization or itineracy at LaAlO₃/SrTiO₃ interfaces: Hole polarons, oxygen vacancies, and mobile electrons. *Phys Rev B* **74**, 035112 (2006).
- 58 Sing, M. *et al.* Profiling the Interface Electron Gas of LaAlO₃/SrTiO₃ Heterostructures with Hard X-Ray Photoelectron Spectroscopy. *Phys Rev Lett* **102**, 176805 (2009).
- 59 Park, J. *et al.* Oxygen-Vacancy-Induced Orbital Reconstruction of Ti Ions at the Interface of LaAlO₃/SrTiO₃ Heterostructures: A Resonant Soft-X-Ray Scattering Study. *Phys Rev Lett* **110**, 017401 (2013).
- 60 Blochl, P. E. Projector Augmented-Wave Method. *Phys Rev B* **50**, 17953-17979 (1994).
- 61 Kresse, G. & Furthmuller, J. Efficiency of ab-initio total energy calculations for metals and semiconductors using a plane-wave basis set. *Comp Mater Sci* **6**, 15-50 (1996).
- 62 Perdew, J. P., Burke, K. & Ernzerhof, M. Generalized gradient approximation made simple. *Phys Rev Lett* **77**, 3865-3868 (1996).
- 63 Yu, L. P., Ranjan, V., Lu, W., Bernholc, J. & Nardelli, M. B. Equivalence of dipole correction and Coulomb cutoff techniques in supercell calculations. *Phys Rev B* **77**, 245102 (2008).
- 64 Heyd, J., Scuseria, G. E. & Ernzerhof, M. Hybrid functionals based on a screened Coulomb potential (vol 118, pg 8207, 2003). *J Chem Phys* **124**, 219906 (2006).
- 65 Persson, C., Zhao, Y. J., Lany, S. & Zunger, A. n-type doping of CuInSe₂ and CuGaSe₂. *Phys Rev B* **72**, 035211 (2005).
- 66 Freysoldt, C. *et al.* First-principles calculations for point defects in solids. *Rev. Mod. Phys.* **86** (2014).

Supplementary Information for “A polarity-induced defect mechanism for conductivity and magnetism at oxide interfaces” by Liping Yu and Alex Zunger

Supplementary Note 1:

The failures of polar catastrophe model

The key argument in favor of the polar catastrophe mechanism is its predicted critical thickness (L_c) of metal-insulator transition. Both electrostatics and the first principles calculations based on density functional theory (DFT) with the generalized gradient approximation (GGA)¹, shown in Fig. S1c lead to an L_c between three and four unit cells^{2,3}. However, these results may be clouded by specific uncertainties: the electrostatic model depends on the choice of the LAO film dielectric constant and LAO/STO band offsets, whereas the GGA calculation suffers from the well-known band gap underestimation problem⁴. To examine this point we have applied the HSE hybrid functional⁵, which predicts correctly the experimental bulk STO band gap of 3.2 eV. We find an L_c of 4-5 uc (Fig. S2c). It is noteworthy that, for $n_{LAO} = 4$ uc, the band gap of the system turns out to be 1.1 eV, suggesting an insulating behavior, contrasting with the experiment where the robust conductivity has been observed at this thickness. Hence, strictly speaking, the defect-free polar catastrophe model cannot explain the L_c either⁶.

In a *defect-free* interface structure, both previous DFT-GGA calculations^{7,8} and our HSE calculation (Fig.S2d) predict a large electric field of 0.19 V/Å in the LAO film of $n_{LAO} < L_c$, which decreases gradually as n_{LAO} increases for $n_{LAO} \geq L_c$, approaching zero only at infinitely thick n_{LAO} . This prediction of the PC model conflicts with experiments, where only very weak residual field has been observed for all investigated n_{LAO} ⁹⁻¹².

Supplementary Note 2:

Thermodynamical equilibrium Fermi energy as a function of LaAlO₃ thickness

Under a given growth condition, the thermodynamic equilibrium E_F is established as a balance of all electrons and holes concentrations contributed by thermal ionization of all considered defects. According to charge neutrality condition¹³, the E_F can be calculated self-consistently from first principles using defect formation energies as inputs.

As seen in the main text, the charge transfer from surface defect to interface defect always cancels the built-in polar field. For the n-type interface below the critical thickness and p-type interfaces at any thickness, all involved defects are deep defects, the resulting equilibrium E_F always sits near the middle of SrTiO₃ band gap. While for n-type interfaces above the critical thickness, the *surface* O vacancies (V_O) form spontaneously. This V_O defect has a donor level higher than the SrTiO₃ conduction band at the interface. The electrons will be transferred from V_O donor level to the SrTiO₃ conduction bands and pins the E_F near the SrTiO₃ valence band minimum.

Supplementary Note 3:

Justification for the thermodynamic equilibrium

The thin film growth is an out of equilibrium process. Our thermodynamic calculations may be still applied. The more detailed justification can be found in Ref [14]. In brief, the calculated

formation energies and defect levels (deep or shallow) in this work are physically meaningful for both equilibrium and non-equilibrium processes. Non-equilibrium implies that once certain high-energy defects form, kinetic barriers may preserve them, even if their concentration exceeds the nominal equilibrium value. However, it should be clear that defects with high formation energy would always be unlikely to form, since a lot of energy needs to be expended in their creation, and the driving force to lowering the energy is large.

Supplementary Note 4:

The formation ΔH of $V_O(S)$ vs LAO film thickness n_{LAO}

The linear decreasing of ΔH of $V_O(S)$ with increasing n_{LAO} can be understood easily from the opposite dipole created by the charge transfer from $V_O(S)$ to the interface.

In a supercell calculation, the formation energy of an oxygen vacancy at LAO surface (denoted as $V_O(s)$ hereafter) is

$$\Delta H = [\mathcal{E}_D^0 + en_{LAO}E'] - [\mathcal{E}_H^0 + en_{LAO}E] + \mu_O, \quad (1)$$

where \mathcal{E}_D^0 and \mathcal{E}_H^0 are the total energies of the supercell structures in the absence of an electric field across the LAO film with and without the vacancy. The second term in each of the brackets corresponds to the electrostatic energy rise due to the presence of internal electric field E' and E in LAO with and without V_O , respectively. In a 2×2 2D supercell considered here the creation of a single $V_O(S)$ leads to zero electric field in LAO ($E' = 0$ for all n_{LAO}).^{8,15,16} Thus, Eq. (1) reduces to $\Delta H = [\mathcal{E}_D^0 - \mathcal{E}_H^0 + \mu_O] - en_{LAO}E$, where the second term can now be viewed as an opposite dipole, which decreases linearly at a rate of eE as n_{LAO} increases. Therefore, the larger the n_{LAO} , the larger the opposite dipole moment that lowers the total energy of the system, and the more energy decrease in ΔH . For $V_O(I)$ defects, which can not create an opposite dipole that lowers the ΔH , the ΔH is thus independent of n_{LAO} and remains high as n_{LAO} increases⁸.

The slope $d\Delta H/dn_{LAO}$ remains same or almost same as $V_O(S)$ defects accumulate gradually. This is because that the built-in polar field is created by the polar *charge* at surface/interface. Microscopically, the electron transfer from “one $V_O(S)$ ” to the “interface” mainly cancels the polar field caused by the “polar charge at this $V_O(S)$ site”, not the “polar field caused by the polar *charge* at other $V_O(S)$ defect sites”. It means that during gradual formation of $V_O(S)$, though the in-plane-averaged electric field is lowered, each $V_O(S)$ to be formed still face the (almost) same polar field to be cancelled by it. Hence, the decrease in ΔH of $V_O(S)$ should be almost same as $V_O(S)$ defects accumulates. ***This thus explains why the metal-insulator transition due to $V_O(S)$ is sharp.***

Supplementary Note 5:

Critical thickness vs oxygen chemical potential

Eq.(1) suggests that the critical L_c can be approximately determined by the ΔH of the interfacial V_O in TiO_2 layer and the electric field E in the defect-free LAO film (from electrostatics), via

$$L_c = [\mathcal{E}_D^0 - \mathcal{E}_H^0 + \mu_O]/eE, \quad (2)$$

which is a function of the oxygen chemical potential μ_O and the built-in electric field in defect-free LAO. Supplementary Figure 1b shows the variation of resulting L_c due to $V_O(S)$ with respect to $\Delta\mu_O$ (i.e., the oxygen chemical potential relative to $1/2O_2$) at $T = 0K$. The

corresponding $\Delta\mu_O$ of current growth conditions ranges from -1.73 to -2.25 eV, where the L_c is found to be between 3.1 and 3.8 uc. The O-rich annealing conditions have $\Delta\mu_O$ ranging from -0.61 to -1.44 eV, where the resulting L_c varies from 4.2 to 5.3 uc. Considering the possible high kinetic barrier associated with the low-temperature annealing, the O vacancies induced during the growth generally may not be completely compensated, and thus it is expected that the actually L_c in the annealed samples be ~ 4 uc, consistent with experiments.

Supplementary Note 6:

Interfacial charge vs. internal electric field in polar film

In absence of externally applied electric field, the electric displacement $D_{STO} = 0$ in SrTiO₃ side, and $D_{LAO} = E + 4\pi P$ in LaAlO₃ side. According to Gauss' law, the external interface charge $Q = D_{LAO} - D_{STO} = E + 4\pi P$. For $E = 0$, $Q = 4\pi P = 0.5$ e per two dimensional unit cell area, which is the maximum. For $E = -4\pi P$, $Q = 0$, which is the minimum, i.e., the case below the L_c within the polar catastrophe model.

Supplementary Figures

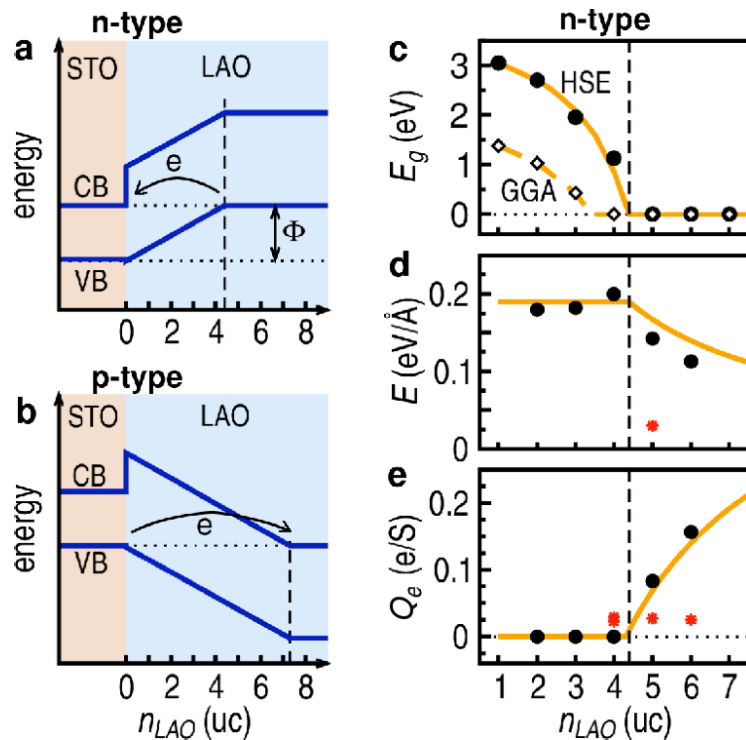


Figure S1: Electronic properties of abrupt defect-free interfaces within the polar catastrophe scenario. **a,b**, schematic band diagram for n-type and p-type interfaces respectively. **c**, GGA and HSE band gaps of 6STO/ n LAO/vacuum interfaces. **d**, Calculated macroscopic planar-averaged electric field in the center of LAO film by HSE. The experimental data (*) is taken from ref.¹⁰. **e**, Calculated interfacial carrier density: HSE (black dots) vs. experiment (red stars)¹⁷. The orange lines in **d,e** are calculated from the simple electrostatic model using $\Phi=3.3$ eV (see **a**) and the LAO film dielectric constant of 30, suggesting a critical

thickness of 4.3 μc for n-type interfaces. Using the same Φ and dielectric constant for p-type interfaces, the resulting critical thickness is 7.3 μc , which is shown in **b**.

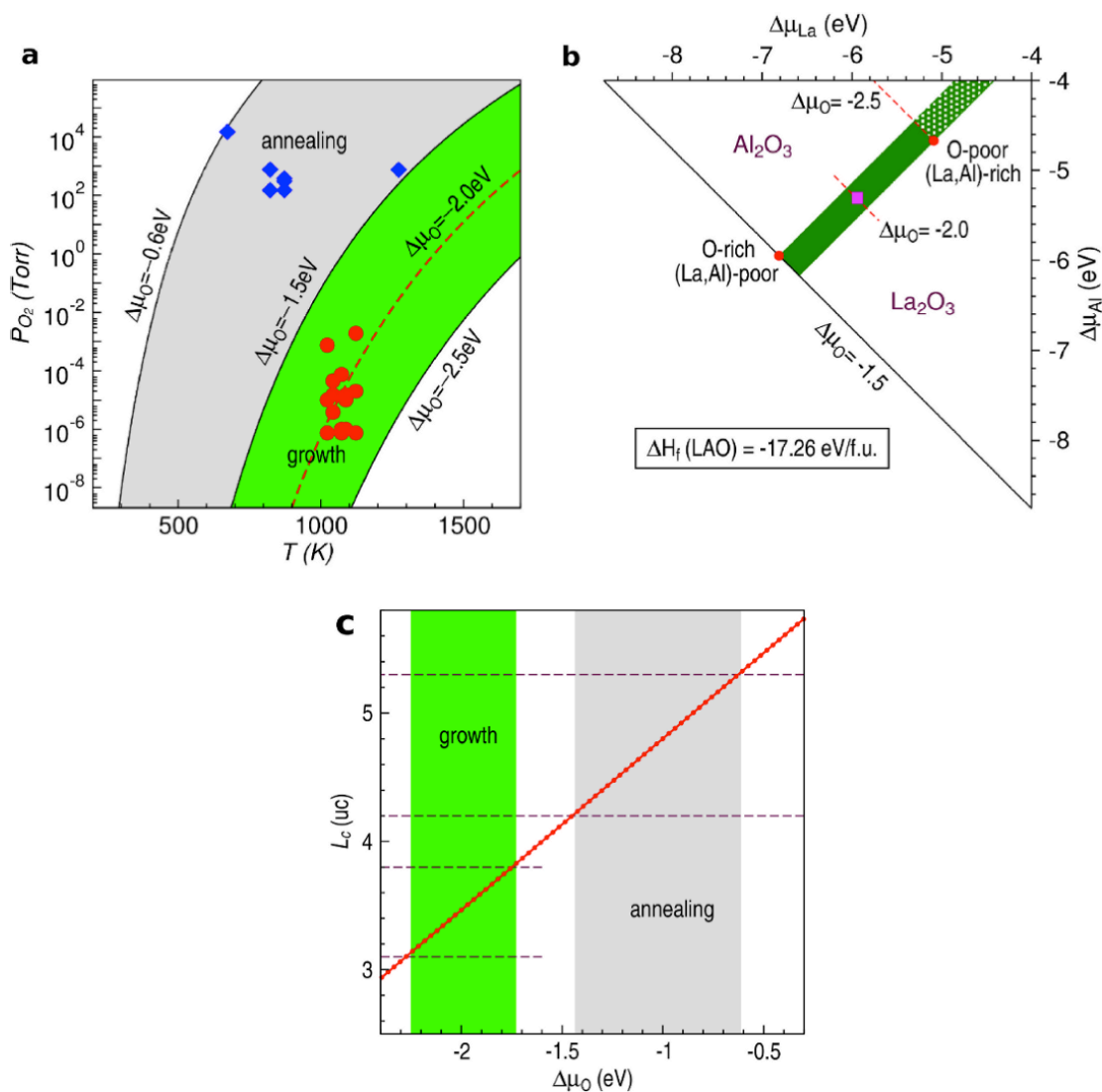


Figure S2: Thermodynamic equilibrium growth conditions and critical thickness for STO/LAO interface. **a**, typical growth (circles) and annealing (diamonds) conditions vs. oxygen chemical potential $\Delta\mu_O$ defined relative to O_2 molecule. The $\Delta\mu_O$ that corresponds to the experimental (P_{O_2} , T) growth conditions was calculated according to the thermodynamic model¹⁸. The red dashed line corresponds to $T = 1050$ K and $P_{O_2} = 6.1 \times 10^{-6}$ Torr, which is referred in Fig.2. **b**, allowed equilibrium chemical potentials (green area) for growing LAO film on top of STO substrate, where the chemical potentials of elements satisfy $\Delta\mu_{La} + \Delta\mu_{Al} + \Delta\mu_O = \Delta H_f = -17.26$ eV and the completing phases (Al_2TiO_5 , $SrAl_2O_4$, La_2TiO_5 , $La_2Ti_2O_7$, $LaTiO_3$, Al_2O_3 , La_2O_3 , SrO , and TiO_2) cannot form. The experimental condition used for Fig.3 refer to $\Delta\mu_O = -2.0$ eV. **c**, the critical thickness (L_c) as a function of O chemical potential used during growth and annealing process.

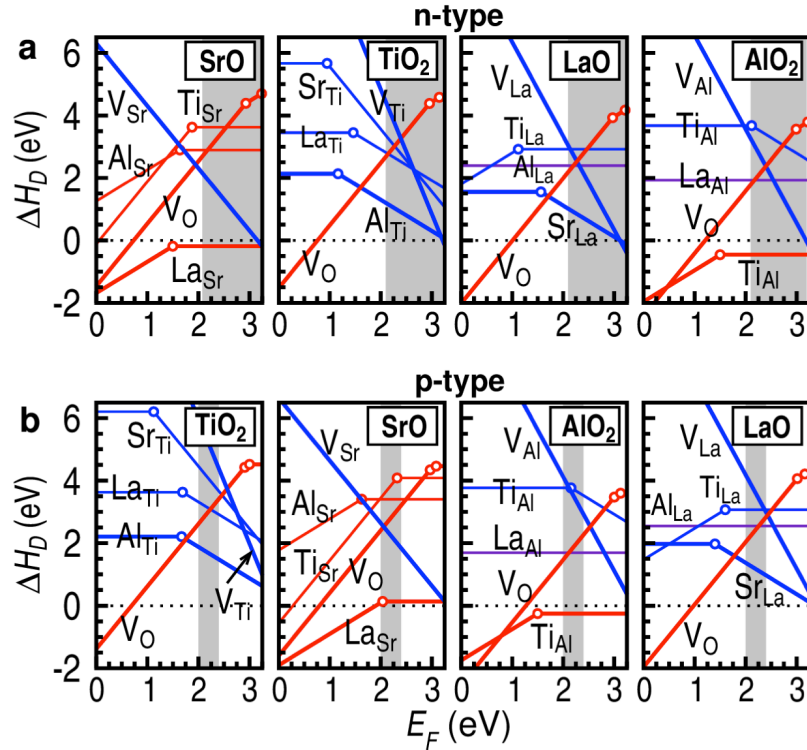


Figure S3: Properties of interfacial defects in the 6STO/2LAO heterostructure containing both n-type and p-type interfaces. a, n-type interface. **b,** p-type interface. Each panel in **a,b** shows various defects in a given atomic layer. Each line represents the ΔH of a donor (red) or acceptor (blue) defect. Different slopes of line segments represent different charge states of a defect that are most stable at given E_F . Open circles mark the defect charge transition energies, i.e., the E_F where the formation energy of a defect in two different charge states equal. The shaded regions in each panel denote the variation range of the equilibrium E_F . The chemical potentials for Sr, Ti, La, Al, and O are -4.36, -6.20, -6.10, -5.46, and -2.0 eV respectively, relative to their corresponding elemental solid or gas phases, which corresponds to $T=1050$ K and $PO_2 = 6.1 \times 10^{-6}$ Torr.

References

- 1 Perdew, J. P., Burke, K. & Ernzerhof, M. Generalized gradient approximation made simple. *Phys Rev Lett* **77**, 3865-3868 (1996).
- 2 Lee, J. & Demkov, A. A. Charge origin and localization at the n-type SrTiO₃/LaAlO₃ interface. *Phys Rev B* **78**, 193104 (2008).
- 3 Reinle-Schmitt, M. L. *et al.* Tunable conductivity threshold at polar oxide interfaces. *Nat Commun* **3**, 932 (2012).
- 4 Perdew, J. P. & Levy, M. Physical Content of the Exact Kohn-Sham Orbital Energies - Band-Gaps and Derivative Discontinuities. *Phys Rev Lett* **51**, 1884-1887 (1983).
- 5 Heyd, J., Scuseria, G. E. & Ernzerhof, M. Hybrid functionals based on a screened Coulomb potential (vol 118, pg 8207, 2003). *J Chem Phys* **124**, 219906 (2006).

- 6 Cossu, F., Schwingenschlogl, U. & Eyert, V. Metal-insulator transition at the LaAlO₃/SrTiO₃ interface revisited: A hybrid functional study. *Phys Rev B* **88**, 045119 (2013).
- 7 Pentcheva, R. & Pickett, W. E. Avoiding the Polarization Catastrophe in LaAlO₃ Overlayers on SrTiO₃(001) through Polar Distortion. *Phys Rev Lett* **102**, 107602 (2009).
- 8 Li, Y., Phattalung, S. N., Limpijumnong, S., Kim, J. & Yu, J. Formation of oxygen vacancies and charge carriers induced in the n-type interface of a LaAlO₃ overlayer on SrTiO₃(001). *Phys Rev B* **84**, 245307 (2011).
- 9 Segal, Y., Ngai, J. H., Reiner, J. W., Walker, F. J. & Ahn, C. H. X-ray photoemission studies of the metal-insulator transition in LaAlO₃/SrTiO₃ structures grown by molecular beam epitaxy. *Phys Rev B* **80**, 241107 (2009).
- 10 Huang, B. C. *et al.* Mapping Band Alignment across Complex Oxide Heterointerfaces. *Phys Rev Lett* **109**, 246807 (2012).
- 11 Slooten, E. *et al.* Hard x-ray photoemission and density functional theory study of the internal electric field in SrTiO₃/LaAlO₃ oxide heterostructures. *Phys Rev B* **87**, 085128 (2013).
- 12 Berner, G. *et al.* Band alignment in LaAlO₃/SrTiO₃ oxide heterostructures inferred from hard x-ray photoelectron spectroscopy. *Phys Rev B* **88**, 115111 (2013).
- 13 Persson, C., Zhao, Y. J., Lany, S. & Zunger, A. n-type doping of CuInSe₂ and CuGaSe₂. *Phys Rev B* **72**, 035211 (2005).
- 14 Van de Walle, C. G. & Neugebauer, J. First-principles calculations for defects and impurities: Applications to III-nitrides. *J Appl Phys* **95**, 3851-3879 (2004).
- 15 Cen, C. *et al.* Nanoscale control of an interfacial metal-insulator transition at room temperature. *Nat Mater* **7**, 298-302 (2008).
- 16 Pavlenko, N., Kopp, T., Tsymbal, E. Y., Mannhart, J. & Sawatzky, G. A. Oxygen vacancies at titanate interfaces: Two-dimensional magnetism and orbital reconstruction. *Phys Rev B* **86**, 064431 (2012).
- 17 Thiel, S., Hammerl, G., Schmehl, A., Schneider, C. W. & Mannhart, J. Tunable quasi-two-dimensional electron gases in oxide heterostructures. *Science* **313**, 1942-1945 (2006).
- 18 Osorio-Guillen, J., Lany, S., Barabash, S. V. & Zunger, A. Magnetism without magnetic ions: Percolation, exchange, and formation energies of magnetism-promoting intrinsic defects in CaO. *Phys Rev Lett* **96**, 107203 (2006).